Continuous-flow sludge settling: a mechanistic 2 x 2 dynamic model, numerical validation and predictions for decision making

Mohand Ouidir Amirat, Jean-Marc Choubert, Françoise Couenne, Christian Jallut, Frédéric Lagoutière, Claire Valentin

Continuous-flow sludge settling: a mechanistic 2 × 2 dynamic model, numerical validation and predictions for decision making

Mohand Ouidir Amirat[a], Jean-Marc Choubert[b], Françoise Couenne[a], Christian Jallut[a], Frédéric Lagoutière[c] and Claire Valentin[a*]

[a] Universite Claude Bernard Lyon 1, CNRS UMR 5007, LAGEPP, 43 Boulevard du 11 Novembre 1918, Bâtiment CPE, Villeurbanne, France

[b] INRAE REVERSAAL, 5 rue de La Doua, Villeurbanne, France

[c] Universite Claude Bernard Lyon 1, CNRS UMR 5208, ICJ, 43 Boulevard du 11 Novembre 1918, Villeurbanne, France

ARTICLE HISTORY

Compiled October 12, 2024

ABSTRACT

The separation of solid particles from the liquid phase is the final operation in an activated sludge wastewater treatment plant. This paper introduces a one-dimensional, knowledge-based dynamic model incorporating both mass and momentum balances, designed for use in the development of a closed-loop controller. The objective of such a future controller would be to regulate both energy consumption and the quality of water discharged from the clarifier. This model is simulated using an explicit Euler time discretization, along with a spatial discretization based on the finite volume method. The fluxes are approximated using the Rusanov scheme, a method particularly suited for handling nonlinear hyperbolic systems that exhibit discontinuities or shock waves.

Simulation results are compared with experimental data, obtained from measuring the sludge blanket (the upper interface of the solid particle zone) during a transient-state experiment in an urban wastewater treatment plant. Additionally, two predictive scenarios are provided to demonstrate the potential of this model as

*Corresponding author. Tel: +33-472-655-347. E-mail: claire.valentin@univ-lyon1.fr. The authors would like to thank the Auvergne-Rhone-Alpes region's Pack Ambition International 2020 program, for their financial support for the C-StaRRE 4.0 project (Grant number 20PACKR-CVALENTIN-6887).

a decision support tool in wastewater treatment processes.

KEYWORDS

Sludge continuous-flow settling process; one-dimensional model; 2x2 hyperbolic partial differential equations system; Comparison of simulated results with experimental data; Predictions.

1. Introduction

A thorough understanding of organic urban sludge settling in wastewater treatment plants is essential for two main reasons: (a) to ensure that the clarified water discharged into the environment meets required quality and environmental standards, and (b) to guide decisions on appropriate closed-loop control strategies that can reduce operating costs (e.g., energy) or improve effluent quality. During the settling process, the solid particles in the sludge gradually settle within the suspension, resulting in the formation of three distinct zones: the upper clarification zone, which contains only liquid; the intermediate zone, where solid particles settle freely with minimal interaction; and the compression zone at the bottom, where solid particles form a concentrated porous bed. In this compression zone, the mass concentration of solid particles exceeds a critical threshold, beyond which interaction forces between particles become significant.

These three zones are separated by two mobile interfaces: the sludge blanket, which marks the boundary between the clarification and intermediate zones, and another interface defined by the critical concentration threshold, which separates the intermediate and compression zones [1–3]. If the clarifier's downstream pump flow rate is too low relative to the upstream sludge flow rate, solid particles may escape from the system at the top, leaving only the two lower zones. In such cases, which are undesirable, the clarification zone disappears entirely.

The literature on settling one-dimensional dynamic modeling (excluding biological reactions) primarily addresses two cases: the batch settler, which is used to study sludge settling properties, and the continuous settler (secondary clarifier) employed in urban wastewater treatment plants. Two types of models are commonly proposed:

highly detailed two-dimensional (2-D) or three-dimensional (3-D) computational fluid dynamics (CFD) models, often used for design purposes (see, for example, [4–6]), and simplified one-dimensional (1-D) models. Since our objective is to develop a model incorporating both mass and momentum balances for designing a closed-loop controller to regulate both energy consumption and water quality at the top of the clarifier, the highly detailed approach is not suitable. Instead, a 1-D model is recommended. In the future, such a 1-D model could also be applied to develop a digital twin, serving as a real-time management tool.

The measurements conducted at a short distance from the center of the clarifier during the experiment described in Section 4 align with the design of a 1-D model. These measurements include the depth of the sludge blanket and concentration measurements at various heights over time. In these vertical settlers, the solid phase moves at a variable velocity within the liquid phase. Consequently, regardless of the 1-D model considered, it must incorporate either a dynamic momentum balance or a constitutive equation to account for velocity variations in both space and time. The literature describes four families of 1-D models:

1. Models based on a dynamic solid particle mass balance coupled with a constitutive equation that defines the solid particle velocity, referred to as the batch or hindered settling velocity [1, 7–12]. G. J. Kynch [13] initiated this approach which was further improved by M.K. Stenstrom [14], Z. Z. Vitasovic [15], I. Takács [11], R. Bürger [1] and S. Diehl [8], without being exhaustive. The double-exponential Takács settling velocity function is frequently used [11]. The state-of-the-art model in this family for wastewater treatment plants (WWTP) is the Bürger-Diehl model, which includes capabilities for handling both compression and dispersion effects [1];
2. Models based on a dynamic solid particle mass balance and a static momentum balance, that defines the flux density function as a constitutive equation [3, 17];
3. Models based on both a dynamic solid particle mass balance and a dynamic momentum balance [2, 18–20]. This approach is more recent due to its two dynamic balances, which are more difficult to process numerically;
4. Models based on both the dynamic solid particle mass and momentum balances,

along with the sludge blanket location as an additional variable, where the variation of the blanket location is governed by a dynamic equation derived from a mass balance [21, 22]. This approach results in a coupled implicit PDE system augmented by an ODE and is currently applied only to batch settling scenarios with zero inlet and outlet flows.

An interesting review of family 1 and 2 clarifier 1-D dynamic models can be found in [23]. In the first family, the models require at least five parameters that need to be calibrated, in the constitutive equations of the Kynch batch flux density function, the compression function and the dispersion functions [1]. In the second family, the models require five parameters that need to be calibrated; in the constitutive equations of flux density function, in the effective solid stress and the critical concentration [3, 17]. The model presented in this paper, which belongs to family 3, requires the calibration of five parameters. This analysis is not exhaustive. Its interest is to provide an indication of the number of parameters that need to be calibrated in the constitutive equations of the various models in the different families. However, any constitutive equation, validated heuristically through experiments, can be used regardless of the number of parameters involved. The review [23] presents tables with various constitutive equations, in particular those related to Kynch batch flux density functions.

These four families of 1-D models are general and encompass a wide range of settling processes, including primary and secondary settling in urban, mining, and coastal zone contexts. Each model requires context-specific adaptation of parameter values. The advantage of family 1 and 2 models is that they yield scalar partial differential equation (PDE) models. In a different approach, family 3 models benefit from a direct derivation from two conservation balances, providing an explicit representation of the four forces acting on solid particles: pressure, effective inter-particle stress, gravity, and drag force. However, family 3 models result in a system of weakly hyperbolic nonlinear PDEs, making their numerical simulation more complex and requiring greater computational resources. Family 4 models consist of coupled implicit PDE systems added with an ODE, and their numerical simulation is as complex as that of family 3 models. In [21], a two-PDEs system derived from both the solid particle mass and momentum balances, along with an ODE representing the variation in the location of the sludge

blanket mobile interface is used (family 4 model). Simulating this model using a centred finite difference numerical scheme produces a sludge blanket descent dynamic that aligns well with the measurements. However, this numerical scheme only captures the change in the average concentration beneath the sludge blanket, as it cannot account for spatial discontinuities or shock waves in certain state variables, such as solid particle volume fraction. Consequently, it is unable to predict the temporal changes in sludge concentration at the bottom or the lowest interface location between the intermediate zone and the compression zone.

This paper is structured as follows: section 2 presents a one-dimensional functional description of the secondary clarifier and a one-dimensional dynamic model belonging to family 3, which describes the behaviour of sludge based on both dynamic mass and momentum balances. This model is a 2x2 hyperbolic PDEs system with nonlinear source terms, associated with constraints specific to two-phase suspensions with non-constant velocity, as well as constitutive equations and boundary conditions. It is simpler than the family 3 model presented in [2], which focuses on sedimentation in a river estuary. Section 3 introduces a numerical scheme specifically designed for this nonlinear hyperbolic system, which can exhibit discontinuities or shock waves. In section 4, an experimental dynamic event is described, and the simulated results obtained using our model are compared with experimental data collected from an urban water treatment plant. Sections 5 and 6 present two predictive simulations of relevant fictitious scenarios during an ongoing storm: one involving a second pump failure and the other with a recirculation flow rate calculated to maintain a constant quantity of particles in the secondary clarifier. Finally, section 7 presents the conclusions and future perspectives for this work.

2. A mechanistic 1-D 2x2 dynamic model

2.1. Clarifier and settling description

Fig. 1 illustrates a 1-D schematic representation of the clarifier (settling tank). If the flow rate of the clarifier's downstream pump is appropriately calibrated in relation to the upstream sludge feed flow rate, clarified water that meets environmental standards

can be released from the top. The contents of the open-air settler can be divided into three aforementioned zones, separated by two interfaces that move in space and time. The levels of these two interfaces are indicative only in this one-dimensional schematic representation and depend on the specific scenarios. They align with the simulations and measurements taken during the dynamic event, in which the sludge blanket rises above the feed level at certain moments. Depending on the scenario, the two interfaces may be situated very close to each other.

- The upper interface represents the sludge blanket, located at depth $z_v(t)$. This interface separates the clarification zone (which contains no solid particles) from the intermediate zone. The sludge blanket is measured using an ultrasound Royce device, positioned on the rotating deck above, which detects the depth at which there is a high gradient of solid particle concentration.
- The lower interface is defined by the intermediate/compression threshold, located at depth $z_c(t)$. At this depth, the behaviour changes as the solid particle concentration $C_s(z,t)$ exceeds the threshold C_c, above which interparticle stress becomes significant. Below $z_c(t)$, the liquid phase flows through the porous network, [27].

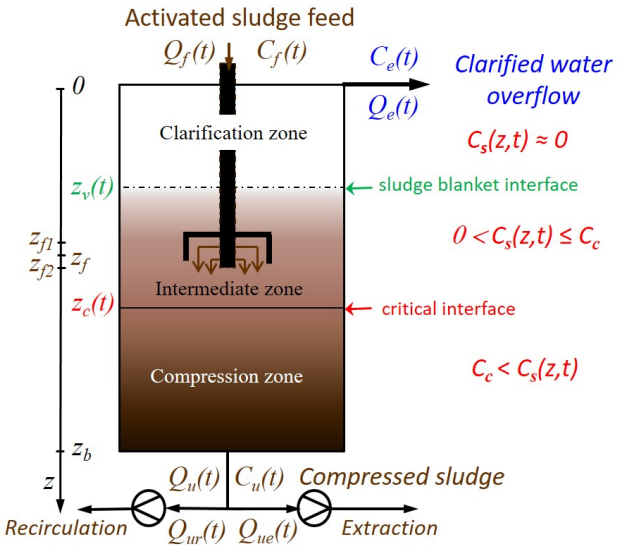

Figure 1.: One-dimensional schematic view of a sludge clarifier including relevant notations about flow rates, concentrations and depths.

The clarifier is connected to the wastewater treatment process at three locations: one

inlet and two outlets:

- one inlet where activated sludge flows into the clarifier by gravity from the upstream biological aeration tank at the volumetric flow rate of $Q_f(t)$ and a solid particle concentration of $C_f(t)$. This activated sludge contains a high quantity of microorganisms, while primary sludge does not. Practically, the activated sludge feed enters through a skirt positioned at a depth of approximately $z = z_f$. This skirt helps orient the particles' motion in the vertical direction. In our model, the inlet velocity is assumed to be vertical only. The momentum and mass flows associated with the inlet are incorporated as source terms in the balance equations (1) to (4),
- one top outlet where clarified water exits at $z = 0$, with a volumetric flow rate of $Q_e(t)$ and a solid particle concentration of $C_e(t)$,
- one bottom outlet where compressed sludge is discharged at $z = z_b$, with a volumetric flow rate of $Q_u(t)$ and a solid particle concentration of $C_u(t)$. A fraction of the compressed sludge is recirculated to the aeration tank at a volumetric flow rate $Q_{ur}(t)$, while another fraction is withdrawn from the clarifier at a volumetric flow rate $Q_{ue}(t)$, such that the total flow rate $Q_u(t)$ satisfies the relationship $Q_u(t) = Q_{ur}(t) + Q_{ue}(t)$.

If the flow rate of the downstream pump is too low compared to the upstream sludge feed flow rate, solid particles may exit the system through the top along with the mixture. Consequently, the content of the open-air settler is divided only into two zones: the intermediate zone and the compression zone, with the clarification zone effectively disappearing. Although this scenario is undesirable, the model of this uncontrolled system must account for this situation to accurately reflect the physical phenomena involved and to ensure proper integration with a closed-loop boundary controller in future applications.

2.2. 1-D general dynamic mass and momentum balances

The objective of this model, based on both mass and momentum balances, is to calculate the temporal changes in the solid particle concentration profile within the clarifier,

as well as the outlet concentrations, $C_e(t)$ and $C_u(t)$, given the activated sludge feed flow rate and concentration, $Q_f(t)$ and $C_f(t)$, along with the compressed sludge outlet flow rate, $Q_u(t)$. Additionally, the sludge blanket level, $z_v(t)$, is a measured variable and corresponds to the spatial position of the maximum gradient in the solid particles concentration, $C_s(z,t)$.

This dynamic model, which describes the behaviour of the sludge suspension in the clarifier, is based on two dynamic mass and momentum balances that can be formulated for the two phases under the following commonly used simplifying assumptions [23]:

1. The liquid and solid phases completely fill the constant volume of the clarifier.
2. There is no biological activity during the settling operation and the suspension is fully flocculated prior to sedimentation, [17].
3. The solid particles are of uniform size and shape, [3, 8, 9].
4. Particle concentration is uniform at a given depth, [8, 9].
5. Vessel wall friction is negligible.
6. The solid particles are small relative to the containing vessel and have the same density, [3].
7. The solid particle and fluid mass densities, ρ_s (kg/m^3) and ρ_l (kg/m^3), are constant, with no mass transfer occurring between the solid and liquid phases, [2, 3, 8, 9].
8. The open-air clarifier has a constant cross-sectional area.

As the liquid and solid phase densities ρ_l and ρ_s are constant, the most natural state variables are the particle (liquid) volume fraction, $\varepsilon_s(z,t)$ $(\varepsilon_l(z,t))$, along with the particle (liquid) flux, $f_s(z,t) = \varepsilon_s(z,t)v_s(z,t)$ $(f_l(z,t) = \varepsilon_l(z,t)v_l(z,t))$, where $v_s(z,t)$ and $v_l(z,t)$ represent the Eulerian average velocities of the solid and liquid phases, respectively. The depth from the top of the clarifier is denoted by z, and the time is represented by t. Consequently, the solid particle mass concentration is expressed as $C_s(z,t) = \rho_s\varepsilon_s(z,t)(kg/m^3)$.

Remark: for the sake of clarity, the notations in the following equations have been simplified by omitting (z,t) when the variables are considered for all z and all

t. Additionally, the following subscript notation is used for the partial derivatives: $\frac{\partial f}{\partial t} = \partial_t f$ *and* $\frac{\partial f}{\partial z} = \partial_z f$.

The sludge feed inlet is represented by an interval centered on z_f with a width of Δz_f. (It allows the representation of different types of skirts that drive the flow of sludge downwards). This area is located between $z_{f2} = z_f + \Delta z_f/2$ and $z_{f1} = z_f - \Delta z_f/2$. The gate (Top-Hat) function, $\Pi(z, z_f, \Delta z_f)$, appears in the source terms related to the sludge feed in the balance equations. This gate function is equal to 1 between z_{f1} and z_{f2} and 0 elsewhere. For simplicity, it is denoted as $\Pi_f(z)$.

The dynamic mass balances for the solid phase and the liquid phase are formulated as follows:

Solid phase mass balance:

$$\partial_t(\rho_s \varepsilon_s) + \partial_z(\rho_s f_s) = \mathrm{f_{1s}}(Q_f, C_f)\Pi_f(z) \tag{1}$$

Liquid phase mass balance:

$$\partial_t(\rho_l \varepsilon_l) + \partial_z(\rho_l f_l) = \mathrm{f_{1l}}(Q_f, C_f)\Pi_f(z) \tag{2}$$

where the discontinuous source terms, $\mathrm{f_{1s}}\Pi_f$ and $\mathrm{f_{1l}}\Pi_f$, represent the activated sludge feed inlet in the solid and liquid mass balance equations, respectively. Both source terms depend on Q_f, the total volumetric flow rate of the feed, and on C_f, the mass concentration of solid particles at the feed inlet, and A, the section of the cylindrical clarifier. Detailed definitions of the discontinuous source terms in the final PDE system are provided in Section 2.5.

Similarly, the dynamic momentum balance equations can be formulated for both the solid phase and the liquid phase, as referenced in [2, 28, 29]:

Solid phase momentum balance:

$$\begin{aligned}\partial_t(\rho_s f_s) &= -\partial_z(\rho_s f_s v_s) + \varepsilon_s\rho_s g - \varepsilon_s\partial_z P - \partial_z\sigma_e(\varepsilon_s) + r(\varepsilon_s)(v_l - v_s) \\ &\quad + \mathrm{f_{2s}}(Q_f, C_f)\Pi_f(z) \end{aligned} \tag{3}$$

where:

$\varepsilon_s\rho_s g$	volumetric gravitational force (body force)
$\partial_z P(z,t)$	gradient of the pore pressure (hydrodynamic pressure)
$\partial_z\sigma_e(\varepsilon_s)$	gradient of the interparticle stress between the solid particles, [17].
$r(\varepsilon_s)(v_l - v_s)$	Stokes-like drag force i.e., liquid/solid dynamic interaction force representing viscous friction between the two phases. Here, $r(\varepsilon_s)$ is the resistance coefficient.

Liquid phase momentum balance:

$$\begin{aligned}\partial_t(\rho_l f_l) &= -\partial_z(\rho_l f_l v_l) + \varepsilon_l\rho_l g - \varepsilon_l\partial_z P - r(\varepsilon_s)(v_l - v_s) \\ &\quad + \mathrm{f_{2l}}(Q_f, C_f)\Pi_f(z) \end{aligned} \tag{4}$$

where $\mathrm{f_{2s}}\Pi_f$ and $\mathrm{f_{2l}}\Pi_f$ are, respectively, the discontinuous source terms that represent the inflow of fluid and solid particles of the activated sludge at the feed inlet, characterized by a specific velocity. This momentum inflow at the feed level must be incorporated into the momentum balance, similar to how the mass input at the feed level is considered in the mass balance. These two terms depend on Q_f, C_f and A.

The next two sections present the specific constraints inherent to a two-phase suspension with non-constant velocity, as well as the constitutive relations for $\sigma_e(\varepsilon_s)$ and $r(\varepsilon_s)$.

2.3. Specific constraints for two-phase suspensions

Since the sludge is a two-phase (liquid and solid) suspension, the sum of the solid particle volume fraction and the liquid volume fraction is given by:

$$\varepsilon_l + \varepsilon_s = 1 \tag{5}$$

Therefore, the liquid volume fraction, $\varepsilon_l(z,t)$, can be easily calculated knowing ε_s.

As solid particles and fluid are considered incompressible, the total volume flux of the suspension (or mixture average volume velocity), denoted $v_m(z,t)$, can be calculated as the sum of the volume fluxes of the two phases. This relationship is expressed by the following equation:

$$v_m = \varepsilon_l v_l + \varepsilon_s v_s \tag{6}$$

Moreover, by applying equation (5), the sum of the two mass balances, (1) for the solid phase and (2) for the liquid phase, each divided by their respective phase densities, results in:

$$\partial_z v_m = \left[\frac{\mathrm{f_{1s}}}{\rho_s} + \frac{\mathrm{f_{1l}}}{\rho_l}\right] \Pi_f(z) \tag{7}$$

This implies that the v_m divergence is zero throughout the clarifier except in the feed zone. The inlet flow is assumed to be uniformly distributed along the vertical feed zone between z_{f1} and z_{f2}, with a constant volumetric flow per unit length. Due to global volume balance, the mean volume velocity v_m takes on specific values in different zones of the clarifier: it is equal to $-Q_e(t)/A$ for depths $z < z_{f1}$ and $Q_u(t)/A$ for depths

$z > z_{f2}$. Within the feed zone, v_m varies linearly, as expressed in equation (8):

$$v_m(z,t) = \begin{cases} -Q_e/A & \text{if } z < z_{f1} \\ \frac{1}{A\Delta z_f}\left[(Q_e+Q_u)z - z_{f1}Q_u - z_{f2}Q_e\right] & \text{if } z_{f1} \leq z \leq z_{f2} \\ Q_u/A & \text{if } z > z_{f2} \end{cases} \tag{8}$$

Thus, by using (5) and (6), the liquid phase velocity v_l can be expressed as a function of the solid volume fraction ε_s, the solid phase velocity v_s and the mixture average velocity v_m:

$$v_l = \frac{v_m - \varepsilon_s v_s}{(1-\varepsilon_s)} \tag{9}$$

Note that this equation is well-defined since liquid occupies the interstices between solid particles throughout the clarifier, ensuring that $\varepsilon_s \neq 1$.

2.4. Constitutive equations

Some quantities, like the interparticle stress, σ_e, and some parameters, such as the drag force resistance coefficient, r, are functions of the solid particle volume fraction ε_s. These quantities are characterized by constitutive expressions, generally derived from experimental data. These expressions are empirical and depend on the specific properties of the sludge. Various constitutive equations have been proposed in the literature for different contexts, such as urban wastewater, mining effluents, estuarine, and coastal zones. A comprehensive overview of these approaches can be found in [23].

The following constitutive equations provided by [3] for $\sigma_e(\varepsilon_s)$ and by [2] for $r(\varepsilon_s)$ are particularly well-suited for modeling the characteristics of urban sludge:

$$\sigma_e(\varepsilon_s, \alpha) = \alpha(\varepsilon_s)\sigma_0 \frac{\varepsilon_s^{n_s} - \varepsilon_c^{n_s}}{\varepsilon_c^{n_s}} \tag{10}$$

$$r(\varepsilon_s) = \frac{\rho_l g}{K(\varepsilon_s)} \text{ with } K(\varepsilon_s) = \frac{A_k}{\varepsilon_s^{2/(3-n_r)}} \tag{11}$$

where σ_0, n_s, A_k and n_r are constant parameters that characterize the sludge, with permeability K (see Table 1 for the values used in simulations). The parameter $\alpha(\varepsilon_s)$ is a piecewise constant parameter defined as follows:

$$\alpha(\varepsilon_s) \quad = \quad \begin{cases} 0 & \text{for } \varepsilon_s \leq \varepsilon_c \\ 1 & \text{for } \varepsilon_s > \varepsilon_c \end{cases} \tag{12}$$

where ε_c is the critical solid volume fraction intermediate/compression threshold. The function $\alpha(\varepsilon_s)$ equals zero in the intermediate zone, where the particles are relatively distant from one another due to low concentration, and equals one in the compression zone, where interparticle stress becomes significant as particles are in closer proximity.

Thus, the constitutive equation for $\sigma_e(\varepsilon_s, \alpha)$ varies according to the zones within the clarifier. The formulation of $\sigma_e(\varepsilon_s, \alpha)$ is selected to be a continuous function at $\varepsilon_s = \varepsilon_c$.

2.5. 1-D sludge continuous settling 2×2 dynamic model

With all these considerations taken into account, the four dynamic balance equations presented in section 2.2 can be expressed only in terms of the solid particle volume fraction, ε_s, and the solid particle volume flux, f_s. This is achieved after applying all the simplifications implied by assumptions 1. to 8. and utilizing the algebraic equations specific to this two-phase suspension established in section 2.3.

Moreover, a simplified expression of the pore pressure gradient can be considered for this system because the settling is very slow and the suspension is at a low concentration. This leads to a pressure profile that is identical to the static gradient due to Archimedes' buoyancy force, expressed as $\partial_z P = \rho_l g$, and remains consistent throughout the duration of the operation, [22]. It constitutes an additional 9th assumption:

9. $\forall z \in [0, z_b]\,, \partial_z P = \rho_l g$.

Then, the solid particle volume fraction ε_s and flux f_s variations can be expressed in

conservative form by manipulating equations (1), (3) and (9), [20], as follows:

$$\partial_t \varepsilon_s + \partial_z f_s = \frac{\mathrm{f_{1s}}(Q_f, C_f)}{\rho_s} \Pi_f(z) \tag{13}$$

$$\begin{aligned} \partial_t f_s + \partial_z \left(\frac{f_s^2}{\varepsilon_s} + \frac{\sigma_e(\varepsilon_s)}{\rho_s} \right) &= \varepsilon_s g (1 - \frac{\rho_l}{\rho_s}) + \frac{r(\varepsilon_s)(\varepsilon_s v_m - f_s)}{\rho_s \varepsilon_s (1 - \varepsilon_s)} \\ &\quad + \frac{\mathrm{f_{2s}}(Q_f, C_f)}{\rho_s} \Pi_f(z) \end{aligned} \tag{14}$$

where:

$$\mathrm{f_{1s}}(Q_f, C_f) = \frac{C_f(t) Q_f(t)}{A \Delta z_f} \tag{15}$$

$$\mathrm{f_{2s}}(Q_f, C_f) = \frac{C_f(t) Q_f^2(t)}{A^2 \Delta z_f} \tag{16}$$

Remark: Most papers in the literature define a model using the state variables (ε_s, v_s) [2, 18, 19, 21, 22]. However, for mathematical developments and numerical considerations, the variables (ε_s, f_s) seem to us to be more appropriate.

The matrix form of the 2×2 PDE model of the urban sludge settling is as follows:

$$\partial_t \boldsymbol{x} + \partial_z \boldsymbol{F_s}(\boldsymbol{x}) = \boldsymbol{\mathcal{S}_1}(\boldsymbol{x}) + \boldsymbol{\mathcal{S}_2} \tag{17}$$

where $\boldsymbol{x}$ represents the state variable vector:

$$\boldsymbol{x} = \begin{pmatrix} \varepsilon_s \\ f_s \end{pmatrix}$$

$\boldsymbol{F_s(x)}$ represents the flux vector:

$$\boldsymbol{F_s(x)} = \begin{pmatrix} f_s \\ \frac{f_s^2}{\varepsilon_s} + \frac{\sigma_e(\varepsilon_s)}{\rho_s} \end{pmatrix} \tag{18}$$

and $\boldsymbol{\mathcal{S}_1(x)}$ and $\boldsymbol{\mathcal{S}_2}$ are the source terms:

$$\boldsymbol{\mathcal{S}_1(x)} = \begin{pmatrix} 0 \\ \varepsilon_s g(1 - \frac{\rho_l}{\rho_s}) + \frac{r(\varepsilon_s)(\varepsilon_s v_m - f_s)}{\rho_s \varepsilon_s (1-\varepsilon_s)} \end{pmatrix}$$

$$\boldsymbol{\mathcal{S}_2} = \begin{pmatrix} \frac{\mathrm{f_{1s}(Q_f, C_f)}}{\rho_s} \Pi_f(z) \\ \frac{\mathrm{f_{2s}}(Q_f, C_f)}{\rho_s} \Pi_f(z) \end{pmatrix}$$

2.6. Boundary conditions

To determine the appropriate boundary conditions, we express the left-hand side of the nonlinear hyperbolic system (17) in quasi-linear form using the Jacobian matrix $\boldsymbol{J(x)}$:

$$\partial_t \boldsymbol{x} + \partial_x \boldsymbol{F_s(x)} \partial_z \boldsymbol{x} = \partial_t \boldsymbol{x} + \boldsymbol{J(x)} \partial_z \boldsymbol{x}$$

where

$$\boldsymbol{J(x)} = \begin{cases} \begin{bmatrix} 0 & 1 \\ \frac{-f_s^2}{\varepsilon_s^2} & \frac{2f_s}{\varepsilon_s} \end{bmatrix} & \text{for } 0 < \varepsilon_s \leq \varepsilon_c \\ \begin{bmatrix} 0 & 1 \\ \frac{-f_s^2}{\varepsilon_s^2} + \frac{\sigma_0 n_s}{\rho_s \varepsilon_c^{n_s}} \varepsilon_s^{n_s - 1} & \frac{2f_s}{\varepsilon_s} \end{bmatrix} & \text{for } \varepsilon_s > \varepsilon_c \end{cases} \tag{19}$$

The spectrum of the Jacobian matrices $\boldsymbol{J(x)}$, denoted $Sp(\boldsymbol{J(x)})$, provides the eigenvalues, λ_J:

$$Sp(J(x)) = \begin{cases} \left\{ \frac{f_s}{\varepsilon_s}, \ \frac{f_s}{\varepsilon_s} \right\} & \text{for } 0 < \varepsilon_s \leq \varepsilon_c \\ \\ \left\{ \frac{f_s}{\varepsilon_s} - \sqrt{\frac{\sigma_0 n_s}{\rho_s \varepsilon_c^{n_s}} \varepsilon_s^{n_s - 1}}, \ \frac{f_s}{\varepsilon_s} + \sqrt{\frac{\sigma_0 n_s}{\rho_s \varepsilon_c^{n_s}} \varepsilon_s^{n_s - 1}} \right\} & \text{for } \varepsilon_s > \varepsilon_c \end{cases} \tag{20}$$

The eigenvalue analysis reveals that the system's spatial characteristics shift at the threshold ε_c. When $0 < \varepsilon_s \leq \varepsilon_c$, the Jacobian matrix has a double positive real eigenvalue, indicating that the upper zone of the system is weakly hyperbolic. In this zone, particles move downward under applied forces without obstruction from particles further downstream. Conversely, if $\varepsilon_s > \varepsilon_c$, the matrix exhibits two distinct real eigenvalues, characterizing the lower zone as strictly hyperbolic. Consequently, the complete system remains weakly hyperbolic overall.

Additionally, since the dimensionless ratio $\frac{f_s}{\varepsilon_s \sqrt{\frac{\sigma_0 n_s}{\rho_s \varepsilon_c^{n_s}} \varepsilon_s^{n_s - 1}}}$ is less than 1 in the compression zone (where $\varepsilon_s > \varepsilon_c$), the two eigenvalues have opposite signs. This implies a downstream-driven regime in this zone, meaning that particle movement is constrained by the particles ahead due to the interparticle stress σ_e.

To specify the boundary conditions, we first recall that during clarifier operation, the upstream activated sludge feed volumetric flow rate, $Q_f(t)$, and concentration, $C_f(t)$, are known and measured. Additionally, the withdrawal (either recirculated or removed) volumetric flow rate at the bottom, $Q_u(t)$ is controlled by the selected pump rate on the downstream pipe. Consequently, the top overflow rate, $Q_e(t)$, is also known, as it follows from the constant sludge volume in the clarifier that $Q_f(t) = Q_u(t) + Q_e(t)$. Using these known quantities, we can deduce the boundary conditions necessary to close this system of weakly hyperbolic first-order PDEs, based on the continuity of the two fluxes.

The continuity of the mass flux of solid particles at the top of the clarifier is expressed

as:

$$Af_s(0,t) = -\varepsilon_s^e(t)Q_e(t) \tag{21}$$

where $\varepsilon_s^e(t)$ denotes the solid particle volume fraction at the very beginning of the top overflow outlet.

The continuity of the solid particle momentum flux at the top of the clarifier is expressed as:

$$A\left(\frac{f_s^2(0,t)}{\varepsilon_s(0,t)} + \frac{\sigma_e(\varepsilon_s(0,t))}{\rho_s}\right) = \frac{\varepsilon_s^e(t)Q_e(t)^2}{A_e} \quad \text{if } \varepsilon_s(0,t) > 0 \tag{22}$$

where A_e is the surface area of the top overflow.
The continuity of the mass flux of solid particles at the bottom of the clarifier is expressed as:

$$Af_s(z_b,t) = \varepsilon_s^u(t)Q_u(t) \tag{23}$$

where $\varepsilon_s^u(t)$ is the solid particle volume fraction at the very beginning of the bottom output pipe.

And the continuity of the solid particle momentum flux at the bottom of the clarifier is expressed as:

$$A\left(\frac{f_s^2(z_b,t)}{\varepsilon_s(z_b,t)} + \frac{\sigma_e(\varepsilon_s(z_b,t))}{\rho_s}\right) = \frac{\varepsilon_s^u(t)Q_u(t)^2}{A_u} \quad \text{if } \varepsilon_s(z_b,t) > 0 \tag{24}$$

where A_u is the cross-sectional area of the downstream clarifier pipe.

The state-space representation of continuous sludge settling in a clarifier is thus formulated by the nonlinear hyperbolic system given in (17) added with the constitutive equations for $\sigma_e(\varepsilon_s, \alpha)$, $r(\varepsilon_s)$ and $\alpha(\varepsilon_s)$ as defined in (10), (11) and (12), respectively.

The algebraic relation for v_m is provided in (8), and the influence of the sludge feed is specified in (15) and (16). The boundary conditions are established in (21), (22), (23) and (24).

Given any initial condition within the physical domain, and applying the boundary conditions stated in (21), (22), (23) and (24), the system has a unique solution that remains within this domain. Consequently, this nonlinear infinite-dimensional state-space model is well-posed.

The simulation uses a numerical scheme specifically designed for such nonlinear hyperbolic systems, which are known to exhibit discontinuities or shock waves.

3. Numerical scheme

The review [23] offers an insightful discussion on numerical schemes developed for nonlinear hyperbolic PDEs, nonlinear parabolic PDEs, and mixed hyperbolic-parabolic PDEs. The numerical scheme applied to the 2×2 nonlinear hyperbolic system in this paper necessarily differs due to the presence of two coupled PDEs and additional source terms. The simulations were conducted using explicit Euler time-discretization along with an efficient numerical scheme specifically designed for hyperbolic and weakly hyperbolic nonlinear PDE systems. This involved a finite volume method spatial-discretization of Godunov type using the Rusanov approximation for the fluxes [24], [26]. Based on the integral form of the balance laws, this approach is particularly effective for simulating fluid mechanics, as well as heat and mass transfer processes. One of its key advantages is its ability to locally preserve balance laws with respect to the fluxes [26].

The state space vector is spatially discretized on a uniform mesh consisting of N_z volumes, each with thickness Δz and a constant cross-sectional area, A. Each volume i lies between an upstream boundary, indexed $i-\frac{1}{2}$, and a downstream frontier boundary, indexed $i+\frac{1}{2}$.

Equation (17) can be expressed in integral form as follows:

$$\int_{i-1/2}^{i+1/2} \frac{d\boldsymbol{x}(\boldsymbol{z},\boldsymbol{t})}{dt} dz = \boldsymbol{F_{i-\frac{1}{2}}}(t) - \boldsymbol{F_{i+\frac{1}{2}}}(t) + \int_{i-1/2}^{i+1/2} (\boldsymbol{\mathcal{S}_1}(\boldsymbol{x}) + \boldsymbol{\mathcal{S}_2})\, dz \tag{25}$$

where $\boldsymbol{F_{i\pm\frac{1}{2}}}(t) = \boldsymbol{F_s}(\boldsymbol{x}(z,t))|_{z=(i\pm1/2)\Delta z}$

Considering that the state variables are uniform within each mesh and are represented by, $\bar{\boldsymbol{x}}_{\boldsymbol{i}}(\boldsymbol{t})$, such that:

$$\bar{\boldsymbol{x}}_{\boldsymbol{i}}(t) = \frac{1}{\Delta z} \int_{i-1/2}^{i+1/2} \boldsymbol{x}(z,t) dz$$

equation (25) can be approximated by:

$$\frac{d\bar{\boldsymbol{x}}_{\boldsymbol{i}}(\boldsymbol{t})}{dt} = \frac{1}{\Delta z} \left(\boldsymbol{F_{i-\frac{1}{2}}}(t) - \boldsymbol{F_{i+\frac{1}{2}}}(t) \right) + \boldsymbol{\mathcal{S}_1}(\bar{\boldsymbol{x}}_{\boldsymbol{i}}) + \boldsymbol{\mathcal{S}_2} \tag{26}$$

where we assume that $\boldsymbol{\mathcal{S}_1}(\bar{\boldsymbol{x}}_{\boldsymbol{i}})$ provides a good approximation for $\frac{1}{\Delta z} \int_{i-1/2}^{i+1/2} \boldsymbol{\mathcal{S}_1}(\boldsymbol{x}) dz$.

Let $\boldsymbol{F^n_{i\pm\frac{1}{2}}}$ denote an approximation of the fluxes $\boldsymbol{F_{i\pm\frac{1}{2}}}(\boldsymbol{t})$ as a function of $\bar{\boldsymbol{x}}^{\boldsymbol{n}}_{\boldsymbol{i}}$ at time t_n.

The equation (26) can therefore be expressed as follows:

$$\frac{\bar{\boldsymbol{x}}^{\boldsymbol{n+1}}_{\boldsymbol{i}} - \bar{\boldsymbol{x}}^{\boldsymbol{n}}_{\boldsymbol{i}}}{\Delta t} = \frac{1}{\Delta z} \left(\boldsymbol{F^n_{i-\frac{1}{2}}}(\bar{\boldsymbol{x}}^{\boldsymbol{n}}_{\boldsymbol{i}}) - \boldsymbol{F^n_{i+\frac{1}{2}}}(\bar{\boldsymbol{x}}^{\boldsymbol{n}}_{\boldsymbol{i}}) \right) + \boldsymbol{\mathcal{S}_1}(\bar{\boldsymbol{x}}^{\boldsymbol{n}}_{\boldsymbol{i}}) + \boldsymbol{\mathcal{S}_2} \tag{27}$$

For hyperbolic systems, special attention is required when selecting these approximations [25], [26]. Here, the Rusanov approximation is chosen because it effectively captures shock waves in the model:

$$\boldsymbol{F^n_{i-\frac{1}{2}}}(\bar{\boldsymbol{x}}^{\boldsymbol{n}}_{\boldsymbol{i}}) = \frac{1}{2} \left(\boldsymbol{F^n_s}(\bar{\boldsymbol{x}}^{\boldsymbol{n}}_{\boldsymbol{i-1}}) + \boldsymbol{F^n_s}(\bar{\boldsymbol{x}}^{\boldsymbol{n}}_{\boldsymbol{i}}) \right) - \frac{w^n_{i-\frac{1}{2}}}{2} \left(\bar{\boldsymbol{x}}^{\boldsymbol{n}}_{\boldsymbol{i}} - \bar{\boldsymbol{x}}^{\boldsymbol{n}}_{\boldsymbol{i-1}} \right) \tag{28}$$

where $w^n_{i-\frac{1}{2}}$ represents the propagation velocity of the fastest wave immediately around the interface $i-\frac{1}{2}$ at t_n. To ensure the stability of this method, the mesh

size must satisfy the Courant-Friedrichs-Lewy (CFL) condition, namely, $|w_s^n \frac{\Delta t}{\Delta z}| < 1$. This propagation velocity, w_s^n, corresponds to the velocity of the fastest wave in the hyperbolic system at t_n and is calculated from (20) [25].

Remark: The Rusanov numerical scheme is also effective for weakly hyperbolic systems, such as (17), and will yield a continuously smooth solution in cases involving a rarefaction wave [26].

The model and numerical scheme developed in the previous sections will be applied in section 4 to simulate an experimental dynamic event for validation purposes, and in section 5 to simulate two hypothetical scenarios, worst-case and closed-loop, to assess if the predicted clarifier behaviour is sufficiently consistent for use as a decision support tool.

4. Simulation of a dynamic event at SYSTEPUR plant

A dynamic event was experimentally applied to a full-scale clarifier located at the SYSTEPUR wastewater treatment plant in Vienne, France [31]. This urban treatment facility features two biological aeration tanks operating in parallel and two secondary clarifiers also running in parallel. Each secondary clarifier is equipped with two ON/OFF pumps for sludge recirculation and two ON/OFF pumps for sludge extraction. In accordance with the control strategy, one or two recirculation pumps are always in operation, while zero, one, or two extraction pumps may also be active. Additionally, there is a third recirculation pump available solely for emergencies. Our experimental study focused on investigating the dynamic evolution of the separation between liquid and sludge particles within the clarifier.

The inlet flow was artificially increased by approximately twofold by redirecting the outlets of the two biological aeration tanks to a single clarifier for a duration of about 8 hours (from t=1:40 to t=9:45). This led to a sudden rise in the flow rate of activated sludge Q_f at the inlet to the secondary clarifier. Continuous monitoring was

conducted for flow rates $Q_f(t)$, $Q_{ur}(t)$ and $Q_{ue}(t)$, the depth of the sludge blanket $z_v(t)$, as well as the particle concentrations $C_f(t)$ and $C_{ur}(t)$. The sludge blanket level was measured using an ultrasound Royce device mounted on the rotating deck above. In this section, the simulated results generated by our model are compared with the experimental data specifically collected to validate the 1-D model.

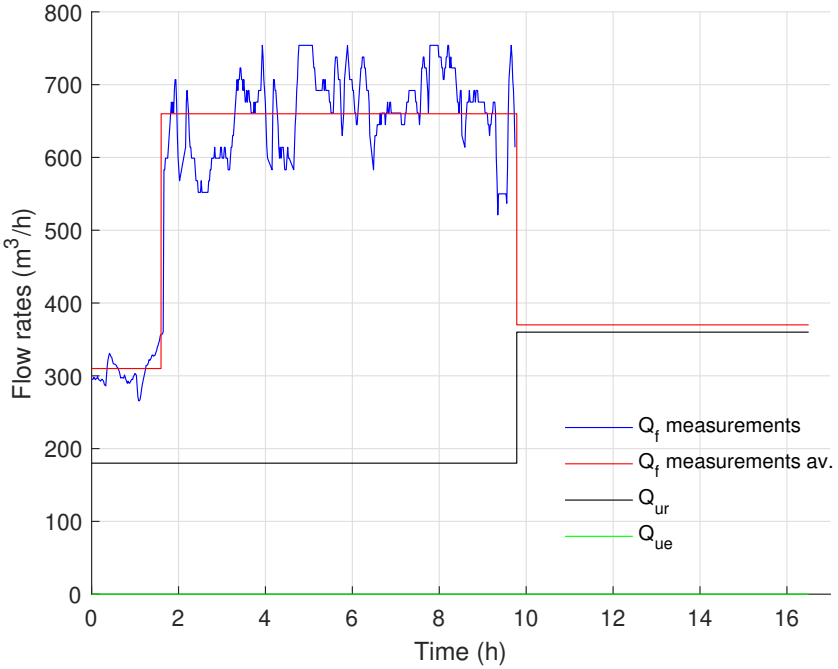

Figure 2.: Measured activated sludge feed flow rate and average value, $Q_f(t)$, recirculation flow rate, $Q_{ur}(t)$ and extraction flow rate, $Q_{ue}(t)$.

During this experimental study, the sludge recirculation flow rate was set at $Q_{ur} = 180\ m^3/h$ until 9:45, utilizing one recirculation pump. Following this time, the recirculation flow rate increased to $Q_{ur} = 360\ m^3/h$, with two recirculation pumps in operation. Throughout the entire duration of the experiment, the sludge extraction flow rate $Q_{ue}(t)$ remained zero. Figure 2 presents the experimental time profile of $Q_f(t)$ along with the average measurements for $Q_f(t)$ and the other flow rate values.

A uniform 200-node spatial mesh, along with the parameter values listed in Table 1, which were selected to align with the measurements, was employed to conduct the simulations. The Chauchat model [2] is part of the same family of models (family

3) as the one presented in this paper, while the Garrido et al. model [3] incorporates a static momentum balance and thus also requires constitutive equations for the forces involved. The corresponding parameter values were determined using the least squares method for a batch sludge settling experiment, and a trial-and-error approach was utilized to fine-tune them for the continuous sludge settling scenario. The flow rate $Q_f(t)$ and the solid particle concentration $C_f(t)$ of the activated sludge at the inlet of the clarifier used in the simulations are averaged values (as represented by the red curve in Fig. 2 and the corresponding value in Table 1).

Some parameter values in Table 1 pertain to the characteristics of the clarifier or

A	1175 m^2	clarifier section
A_k	9.81 10^{-4} m/s	$*C$
C_c	4.18 kg/m^3	$*E$
C_f	2.83 kg/m^3	averaged feed concentration
Δt	1 s	numerical time discretization
Δz	10 cm	numerical spatial discretization
Δz_f	10 cm	feed zone height
ε_c	4.1 10^{-3}	$*E$
n_r	2	$*C$
n_s	11	$*G$
ρ_s	1030 kg/m^3	$*E$
ρ_l	1000 kg/m^3	liquid density
σ_0	0.5 kg/ms^2	$*G$
z_b	2.8 m	clarifier height
z_f	1.8 m	central location of the feed zone

**G: determined by fitting the measurements to the constitutive equations from [3]*
**C: determined by fitting the measurements to the constitutive equations from [2]*
**E: determined by fitting the measurements to our model*

Table 1.: Model parameter values.

to the numerical discretization. The other parameter values are derived from the measurements and ranges suggested in [2] and [3], which have been adapted from mineral to organic sludge. Notably, the density of mineral particulate systems is approximately twice that of organic sludge, which significantly alters the settling dynamics due to the differences in the forces exerted on the solid particles.

Fig. 3 presents the simulated and measured values for the sludge blanket level, which are in close agreement. This figure indicates that, immediately after the dynamic event was applied at the inlet of the clarifier at t=1:40, the sludge blanket level,

481 $z_v(t)$, increases to a depth of 0.48 m by 9:40. At this point, the activation of a second
482 recirculation pump leads to a decrease in the sludge blanket level until the end of the
483 measurement period. This observation suggests that the model effectively captures the
key settling phenomena occurring within the clarifier.

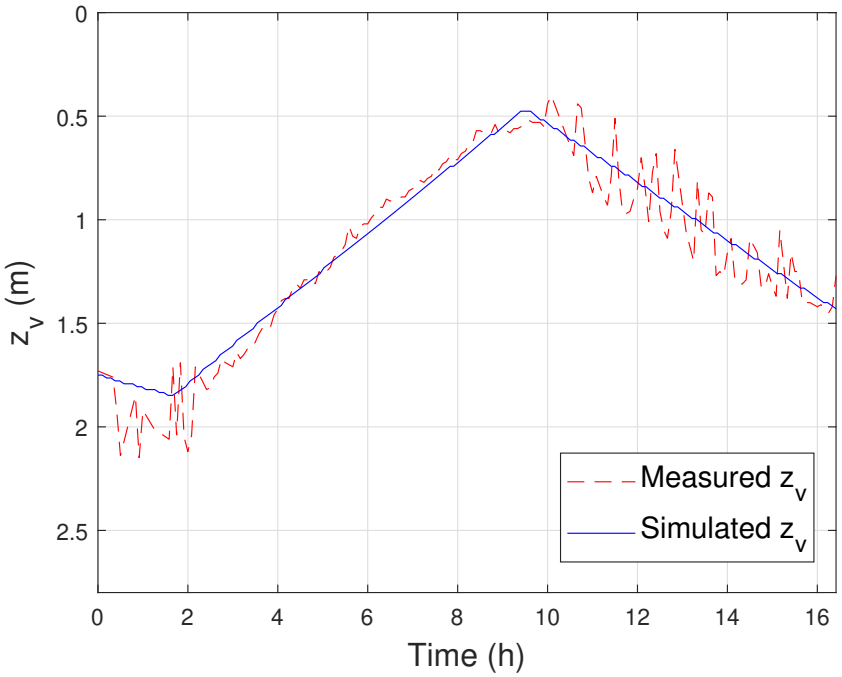

Figure 3.: Comparison of simulated and measured sludge blanket levels, $z_v(t)$, in the dynamic event scenario.

484

485 It is noteworthy that the measurement of the sludge blanket exhibits minimal noise
486 during upward movement; however, it becomes more noisy when moving downwards.
487 This phenomenon occurs because sludge particles do not all descend at the same
488 velocity or in the same manner, and the sensor detects the highest particles. The
489 simulation using the one-dimensional model represents average behaviour.

490

491 Five simulated solid particle concentration spatial profiles (from $t1$ to $t5$) of the
492 dynamic event are presented in Fig. 4.a. For each of these spatial profiles, the particle
493 concentration at the top of the clarifier, $C_s(0,t)$, approaches zero. The spatial profiles
494 show a sharp increase at the depth of the sludge blanket, followed by a more gradual
495 rise as the critical concentration threshold, C_c (indicated by the red dashed line), is

surpassed. Similar to the experimental observations, a change in behaviour is observed below the lower interface when the compression threshold is exceeded, due to the presence of interparticle stress. This results in a higher concentration of solid particles in the lower compression zone. The sludge blanket level corresponds to the spatial position of the maximum concentration gradient of the solid particles. It also corresponds to the location of the shock wave (discontinuity). It should be mentioned that there is no intermediate zone present in this continuous settling process. Five simulated solid

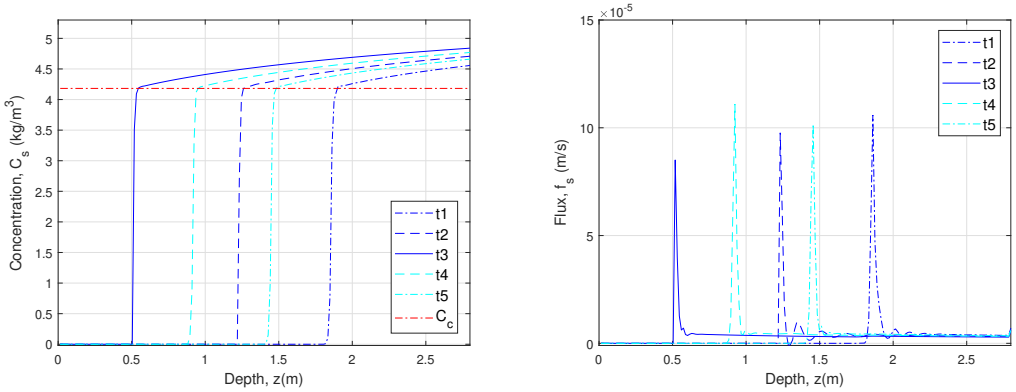

(a) $C_s = \rho_s \varepsilon_s$ (b) f_s

Figure 4.: Simulated state variables vertical spatial profiles at 5 timepoints. (Blue curves: the sludge blanket rises, cyan curves: the sludge blanket descends.)

particle flux spatial profiles (from $t1$ to $t5$) of the dynamic event are shown in Fig. 4.b. The particle flux at the bottom of the clarifier, $f_s(z_b, t)$, is approximately 2.9 10^{-6} m/s. The sludge blanket level corresponds to the spatial position of the maximum flux peak, which reaches around 9 10^{-5} m/s, approximately 30 times the flux at the bottom, $f_s(z_b, t)$. This indicates the location of the shock wave for the solid particle flux variable.

Currently, the runtime for a simulation on a workstation equipped with Intel Xeon processor at 3.8 GHz is 11 min. While this duration may seem lengthy, it can be attributed to the inherently slow nature of the settling phenomenon. Additionally, the numerical scheme must effectively capture the variations in the position of the sludge blanket, which represents a concentration discontinuity.

The model presented in section 2. and validated with measurements in section 4.2.

is now available for predicting clarifier behaviour in various scenarios.

5. Predictive simulation assuming ongoing storm and second pump failure

In this section, we simulate two scenarios: first, the effects of a prolonged storm, and second, the consequences of the second pump failing at 9:45 (worst-case scenario). The aim of these simulations is to evaluate whether the proposed model, along with its boundary conditions, can predict consistent clarifier behaviour. In a real-world scenario, if the second pump were to fail, the operator would start an emergency pump to ensure the proper recirculation flow upon receiving an alarm. Thus, this scenario represents a hypothetical situation.

Flow rates are illustrated in in Fig. 5.a, where ($Q_f(t)$ remains constant at 660 m^3/s instead of experiencing a drop, and $Q_{ur}(t)$ stays at 180 m^3/s). The predicted evolution of the sludge blanket level over time is presented in Fig. 5.b. Five predicted solid particle concentration spatial profiles (from $t1$ to $t5$) are shown in Fig. 6.a, while the predicted concentration at the top of the clarifier is illustrated in Fig. 6.b. It is noteworthy that solid particles would begin to be discharged through the overflow starting at 12:15, with a concentration of 1.94 kg/m^3, three hours after the failure began. Thus, the proposed model with its boundary conditions effectively represents the potential for particles to exit the top of the clarifier when faced with inadequate management strategies.

6. Predictive simulation assuming ongoing storm with recirculation flow rate calculated to maintain particles quantity in the clarifier

In this second predictive scenario, assuming an ongoing storm (with the flow rate $Q_f(t)$ consistent with section 5), we aim to investigate the effects of adjusting the recirculation flow rate, Q_{ur}, to be dependent on the concentrations at the top and bottom of the clarifier, as well as on the feed concentration and flow rate. The relationship is defined

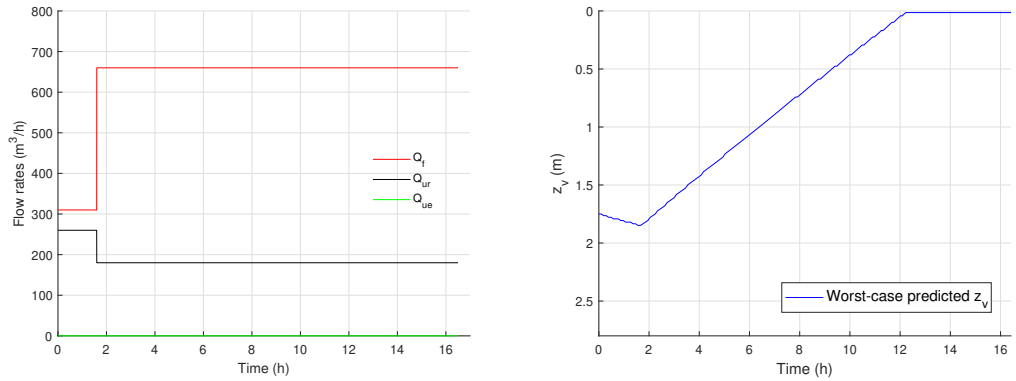

(a) $Q_f(t)$, $Q_{ur}(t)$ and $Q_{ue}(t)$ flow rates (b) Sludge blanket level, $z_v(t)$

Figure 5.: Flow rates and sludge blanket level prediction in case of ongoing storm and 2nd pump failure at 9:45 (worst-case scenario).

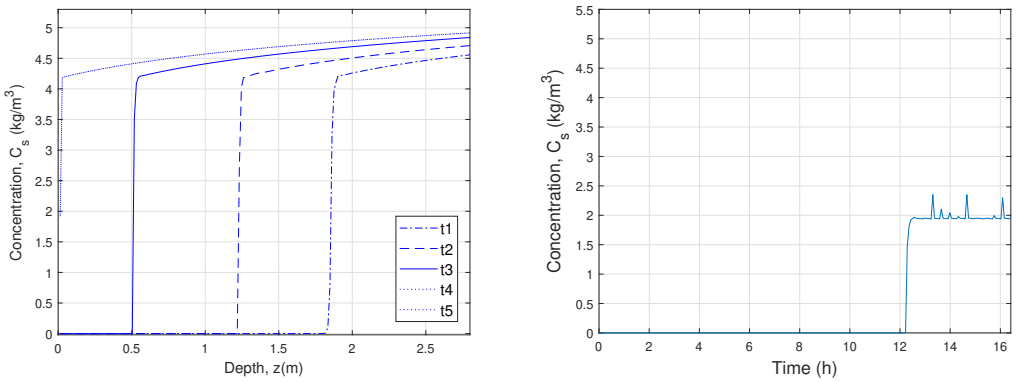

(a) C_s vertical spatial profiles at 5 timepoints (b) Concentration at the top of the clarifier

Figure 6.: Predicted solid particle concentration C_s in case of ongoing storm and 2nd pump failure at 9:45 (worst-case scenario).

as follows: $Q_{ur}^{n+1} = \min\left(\frac{(C_f - \rho_s \bar{\varepsilon}_{s_1}^n)Q_f}{\rho_s(\bar{\varepsilon}_{s_N}^n - \bar{\varepsilon}_{s_1}^n)}, Q_{urmax}\right)$ where index 1 refers to the top of the clarifier and index N to the bottom. This formulation aims to stabilize the sludge blanket at a specific depth. Implementing this requires a variable-flow pump in good working condition (without failures) and appropriate concentration and flow sensors, such as total suspended solids (TSS) optical probes or soft TSS sensors.

The flow rates Q_f and Q_{ue}, representing the scenario, along with the calculated flow rate, Q_{ur}, are illustrated in Fig. 7.b. It can be observed that two pumps are operating, yielding a total flow rate of approximately 410 m^3/s. The predicted evolution of the sludge blanket level over time is presented in Fig. 7.a. We can observe that the sludge

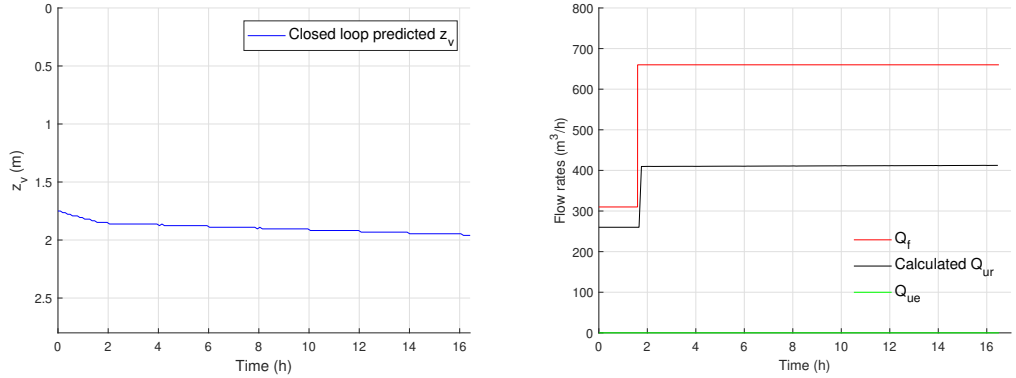

(a) Sludge blanket level, $z_v(t)$ (b) $Q_f(t)$, $Q_{ur}(t)$ and $Q_{ue}(t)$ flow rates

Figure 7.: Sludge blanket level prediction and calculated Q_{ur} flow rate assuming ongoing storm and recirculation flow rate calculated from top and bottom particles volume fractions and feed concentration and flow rate.

blanket level is gradually moving down instead of remaining constant. This behaviour is attributed to a slightly altered distribution of solid particles in the lower part of the clarifier beneath the sludge blanket.

7. Conclusions and perspectives

To the best of our knowledge, the mechanistic one-dimensional dynamic model of urban sludge settling in a continuous secondary clarifier presented in this paper, along with the numerical scheme, is the only model-numerical scheme combination in family 3 specifically designed for urban sludge. Its originality and advantages lie in the fact that both mass and momentum balances are dynamic, explicitly accounting for the four forces acting on the solid particles: pressure, effective inter-particle stress, gravity and drag force. The numerical scheme used for the simulation is designed to address the specific requirements of 2×2 hyperbolic and weakly hyperbolic nonlinear PDEs systems with source terms. It uses a finite volume method for spatial-discretization combined with the Rusanov approximation of the fluxes [26]. This scheme calculates all necessary variables for making operational decisions regarding the clarifier, including the evolution of the solid particle concentration profile over time as well as the outlet concentrations $C_e(t)$ and $C_u(t)$ and sludge blanket position $z_v(t)$, given the activated sludge feed flow rate and concentration $Q_f(t)$ and $C_f(t)$, as well as the compressed sludge outlet flow rate

$Q_u(t)$.

This numerical scheme effectively captures the two mobile interfaces that develop between the three zones during the sludge settling process. To ensure its stability, it is essential to calculate the propagation velocity of the fastest wave in the system, as this value is used to define the time steps in accordance with the Courant-Friedrichs-Lewy (CFL) condition. It should be noted that simulating the 2x2 hyperbolic system, including nonlinear source terms, is more challenging and requires greater computational effort than the simulation of models from families 1 and 2, which is a disadvantage. Future comparative studies could be conducted to quantify the differences in predictions when considering the three families of models for continuous sludge settling.

This paper also presents comparisons with experimental data collected from an urban water treatment plant during a dynamic event, showing that the simulations capture the main settling phenomena within the clarifier. Additionally, this paper presents predictions for two relevant scenarios that differ from the validation scenario and are realistic. The 1-D model proposed here will be used in future works for the design of a closed-loop controller focused on regulating energy consumption and water quality at the top of the clarifier, ultimately contributing to real-time computer-aided management.

Additionally, a decision support tool based on family 3 models will be more effective if it incorporates periodic parameter estimation to adapt to the variability of sludge (primary, secondary, from mines, cities, etc.) and atmospheric conditions. It should also be noted that estimating the parameters of the presented dynamic model to align with the measurements provides an indirect method for determining the intermediate/compression threshold, C_c.

Notations

Index i stands for liquid phase (l) or solid phase (particles) (s).

$\alpha(\varepsilon_s)$	piecewise constant intermediate/compression zone flag
A	cylindric clarifier section (m^2)
$A_e(t)$	overflow surface (m^2)
A_u	outlet pipe section (m^2)
$C_i(z,t)$	solid (liquid) phase mass concentration (kg/m^3) $C_i(z,t) = \rho_i \varepsilon_i(z,t)$
$C_f(t)$	mass concentration of solids at the activated sludge feed (kg/m^3)
$\varepsilon_i(z,t)$	solid (liquid) phase volume fraction
ε_c	solid volume fraction intermediate/compression zone threshold
$f_s(z,t)$	system average volumetric flux (m/s)
$P(z,t)$	excess pore pressure (Pa)
$Q_f(t)$	volumetric flow rate of the activated sludge feed (m^3/s)
$Q_e(t)$	volumetric flow rate of the clarified water released at the top of the clarifier (m^3/s)
$Q_u(t)$	volumetric flow rate of the compressed sludge which is pumped from the bottom of the clarifier (m^3/s)
$r(\varepsilon_s)$	resistance coefficient of the drag force proposed by Darcy and Gersevanov in a two-phase model ($kg.m^{-3}.s^{-1}$)
ρ_i	solid (liquid) phase density (kg/m^3)
$\sigma_e(\varepsilon_s)$	effective solid stress function (Pa)
$v_i(z,t)$	solid (liquid) phase average velocity (m/s)
$v_m(z,t)$	volume average velocity (total volume flux of the suspension) (m/s)
z_b	cylindric clarifier height (m)
$z_c(t)$	intermediate/compression interface location (m)
z_f	average location of the activated sludge feed zone (m)
$z_v(t)$	sludge blanket location (m)

Funding

Supported by the Auvergne-Rhone-Alpes region's Pack Ambition International 2020 program, along with the C-StaRRE 4.0 project (Grant number 20PACKR-CVALENTIN-6887).

Acknowledgements

The authors would like to thank Catherine Cadet from the GIPSA-Lab for her valuable initial inputs.

References

[1] R. Burger, S. Diehl, S. Farâs, I. Nopens, and E. Torfs, *A consistent modelling methodology for secondary settling tanks: a reliable numerical method.* Water Science & Technology, Vol. 68.1, (2013), pp. 192–208.

[2] J. Chauchat, S. Guillou, D. Pham van Bang and K. Dan Nguyen, *Modeling sedimentation-consolidation in the framework of a one-dimensional two-phase flow model*, Journal of Hydraulic Research, 51 (3), K. (2013), pp. 293-305.

[3] P. Garrido, F. Concha, R. Burger, *Settling velocities of particulate systems: 14. Unified model of sedimentation, centrifugation and filtration of flocculated suspensions.* Int. J. Mineral Processing, vol. 72, (2003), pp.57-74.

[4] S. Conserva, F. Tatti, V. Torretta, N. Ferronato, P. Viotti, *An integrated approach to the biological reactor-sedimentation tank system*, Resources, 8(2), (2019), pp. 94-113.

[5] O. Flamant, A. Cockx, V. Guimet, Z. Doquang, *Experimental analysis and simulation of settling process*, Trans. IChemE, Part B, Process Safety and Environmental Protection, 82(B4), (2004), pp. 312–318.

[6] G. Xu, F. Yin, Y. Xu, H-Q Yu, *A force-based mechanistic model for describing activated sludge settling process*, Water Research, 127 (2017), pp. 118-126.

[7] J. P. Chancelier, M. C. De Lara, C. Joannis and F. Pacard. *New insights in dynamic modeling of a secondary settler—II. Dynamical analysis.* Water Research, vol. 31(8), (1997), pp. 1857-1866.

[8] S. Diehl, *On boundary conditions and solutions for ideal clarifier - thickener units*, Chem-

ical Engineering Journal, 80, (2000), pp.119-133.

[9] R. David, P. Saucez, J.L. Vasel and A. Vande Wouwer *Modeling and numerical simulation of secondary settlers: A method of Lines strategy*, Water Research, vol. 25.43, (2009), pp. 319 - 330.

[10] I. Queinnec and D. Dochain, *Modelling and simulation of the steady-state of secondary settlers in wastewater treatment plants*. Water Sci. Technol., vol. 43 (7), (2001), pp.39-46.

[11] I. Takacs, G.G. Party, D. Nolasco, *A dynamic model of the clarification thickening process. Water Research*, vol. 25(10), (1991), pp. 1263-1271.

[12] E. Torfs, Locatelli, Florent, S. Balemans, J. Laurent, P. A. Vanrolleghem, R. Bürger, S. Diehl, P. François, R. Mosse, and I. Nopens, *Concentration-driven models revisited: Towards a unified framework to model settling tanks in WWTPs*, 5th IWA/WEF Wastewater Treatment Modelling Seminar (WWTmod2016), (2016), pp. 109-118.

[13] G. J. Kynch, *A theory of sedimentation*. Trans. Faraday Soc. 48, (1952) pp. 166–176.

[14] M.K. Stenstrom, *A dynamic model and computer compatible control strategies for wastewater treatment plants*, PhD thesis of Clemson University, USA, 1976, pp. 1-322.

[15] Z. Vitasovic, *Continuous settler operation: a dynamic model*. Dynamic Modeling and Expert Systems in Wastewater Engineering. Lewis Publishers, Inc., Chelsea Michigan, (1989), pp. 59-81.

[16] H. Stehfest, *An operational dynamic model of the final clarifier*, Transactions of the Institute of Measurement and Control vol.6(3), (1984), pp. 160-164.

[17] R. Burger, *Phenomenological foundation and mathematical theory of sedimentation-consolidation processes*, Chemical Engineering Journal, vol. 80, (2000), pp.177-188.

[18] C. Valentin, D. Dochain, C. Jallut and V. Dos Santos Martins, *Representation of a Continuous Settling Tank by Hybrid Partial Differential Non Linear Equations for Control Design*, in Proc. World congress IFAC 2020, Berlin, Germany, (2020), 6 pages.

[19] C. Valentin, N. Chassin, F. Couenne, J.M. Choubert and C. Jallut, *1-D Dynamic knowledge-based model of urban sludge continuous-flow settling process. Comparison with experimental results*, Internal report in open access on HAL, (2022), 18 pages.

[20] C. Valentin, F. Lagoutière, J.-M. Choubert, F. Couenne, C. Jallut, *Knowledge-based model and simulations to support decision making in wastewater treatment processes*. Computer Aided Chemical Engineering, Editor(s): Antonios C. Kokossis, Michael C. Georgiadis, Efstratios Pistikopoulos, Elsevier, Vol. 52, (2023), pp. 703-708.

[21] C. Valentin, F. Couenne, C. Jallut, J.M. Choubert and M. Tayakout-Fayolle, *Dynamic*

Modeling of a Batch Sludge Settling Column by Partial Differential Non-Linear Equations with a Moving Interface. in Proc. ADCHEM 2021, 11th IFAC symposium on Advanced Control of Chemical Processes, Venice, (2021), 6 pages.

[22] S.C.A. França, G. Massarani and Jr. E.C. Biscaia, *Study on batch sedimentation simulation – establishment of constitutives equations*, Powder Technology, Vol. 101, Issue 2, (1999), pp.157-164.

[23] B. Li and M.K. Stenstrom, *Research advances and challenges in one-dimensional modeling of secondary settling Tanks - A critical review*, Water Research, vol. 65, 2014, pp. 40-63.

[24] E. Godlewski, P.A. Raviart, *Numerical Approximation of Hyperbolic Systems of Conservation Laws*, Applied Mathematical Sciences Springer, vol. 118, (1996).

[25] R. LeVeque, *Nonlinear Conservation Laws and Finite Volume Methods*, Springer, Berlin, Heidelberg, 1998.

[26] R. LeVeque, *Finite volume methods for hyperbolic problems*, Cambridge university press, vol. 31, 2002.

[27] E. A. Toorman, *Sedimentation and self-weight consolidation: general unifying theory*, Geotechnique, 46, (1996), pp. 103-113.

[28] D. A. Drew, *Mathematical Modeling of two-phase flow*, Technical Summary Report n° 2343, 51 pages, Mathematics Research Center, University of Wisconsin – Madison, USA, 1982.

[29] M. Martin, M. Hoyos and D. Lhuillier, *Sedimentation equilibrium of suspensions of colloidal particles at finite concentrations*, Colloid & Polymer Science, (1994), 272, pp. 1582-1589

[30] G. Bastin, and J. M. Coron, *Stability and boundary stabilization of 1-d hyperbolic systems*, Vol. 88, Basel: Birkhäuser, 2016.

[31] Systepur, *Station Vienne Sud: Présentation de la Station de Traitement des Eaux Usées*, Vienne Condrieu Agglomération Leaflet, 2018.